communications earth & environment

A Nature Portfolio journal

Article

https://doi.org/10.1038/s43247-025-02441-8

Impact-induced mixing generated the stratified soils of the Lunar South Pole Aitken Basin

Haijun Cao, Jian Chen, Xuejin Lu, Jiaqi Kong, Le Qiao, Chengxiang Yin, Changqing Liu, Hongkun Qu, Xiaohui Fu, Yanqing Xin & Zongcheng Ling

The Mg-pyroxene annulus in the South Pole–Aitken (SPA) basin holds crucial information about the lunar crustal evolution, yet its mineralogy and origin remain debate. Here we analyzed the mineralogy, exogenic ejecta, and soil evolution of the 2.8-billion-year-old Chang'e-6 samples from the SPA basin by Raman spectroscopic technique. The Chang'e-6 soils contain mare basalts and noritic exogenous ejecta (31–40 vol%), likely from Chaffee S crater. The derived mineralogy (63–67 vol% plagioclase and 25–27 vol% low-Ca pyroxene) of Mg-pyroxene annulus indicates a ferrous noritic lithology, attributed to a mixture of differentiated norite from the SPA impact melt sheet and re-deposited SPA crust (61–63 vol%). Ejecta accumulation facilitated glass formation, while small impacts induced quartz metamorphism, mixing mature basaltic soil with fresh ejecta, and leading to the fine-grained CE-6 soil. These findings provide new insights into the origin of SPA mafic anomalies and farside mare soil evolution.

The South Pole-Aitken (SPA) basin is the largest and oldest impact basin on the Moon, with a highly unique chemical composition. Compared to typical feldspathic highland terrains, it has higher concentrations of iron and thorium (>7 wt% FeO and 2–3 ppm Th) and is enriched in mafic minerals[1–4], preserving information about early geologic history of the Moon and the constitution of the lunar interior. The formation of the SPA basin is thought to have excavated the lunar interior and exposed deep materials (lower crust or mantle)[5]. Remote sensing observations indicate that the basin floor is primarily composed of pyroxenes, with rare outcrops of olivine[3,6]. Additionally, small-scale, scattered mare basalt plains (3.8–1.7 Ga) are developed within the SPA basin[7], leading to speculation about the origin of young volcanic activity on the lunar farside. Based on the distribution of pyroxene compositions, the SPA can be divided into SPA compositional anomaly, Mg-pyroxene annulus, heterogenous annulus, and SPA exterior[8]. Mg-pyroxene annulus may be related to the thermal effects of the SPA impact event, partial melting of the lunar mantle and the recrystallization of the lunar crust, and multi-stage volcanic activity[9–11]. However, there is no consensus on the mineral composition and formation mechanisms of Mg-pyroxene annulus.

In June 2024, the Chang'e-6 (CE-6) mission successfully landed on the southern mare plain (153.9856°W, 41.6383°S) of the Apollo basin, located within the SPA basin on the lunar farside[12]. The mission returned 1935.3 g lunar soil samples, including both surface and drill core samples[13]. The landing site is situated on an Eratosthenian-aged and moderate-to-high titanium mare unit, characterized by a composition of 6.2 wt% TiO_2, 18.3 wt % FeO, 1.8 ppm Th[14], and minerals consisting of 39.3 vol% plagioclase, 33.8 vol% clinopyroxene, 23.3 vol% orthopyroxene, and 3.6 vol% olivine[15]. The basalt layer has an average thickness of approximately 84 meters and is dated at roughly 2.8 Ga[16], making it one of the youngest basalt units on the lunar farside[7]. The CE-6 zone has experienced significant lateral transport of lunar crustal materials from various source regions[15,17], especially for the Chaffee S crater located at the Apollo basin floor. The returned CE-6 lunar soils provide an opportunity to understand the composition and origin of the Mg-pyroxene annulus.

The lunar regolith is formed by the continuous bombardment of meteorites, micrometeoroids, and solar wind, resulting in a mixture of rock and mineral fragments with various types of glass, most of which are smaller than 1 mm in size[18]. Apollo soils have revealed significant variations in mineral abundance and chemical composition across different regions of the lunar surface[19], highlighting the prolonged crustal reworking and mixing of various components. These differences also indicate that lunar soils have experienced distinct evolution pathways[20]. This work provides a detailed examination of the mineralogy, exogenic ejecta, and impact history of the CE-6 lunar soils (Supplementary Fig. 1), shedding light on secondary magmatic processes that might have occurred on the Moon (i.e., large-scale igneous differentiation that may have taken place within large multi-ring basins and late-stage mare

Shandong Provincial Key Laboratory of Optical Astronomy and Solar-Terrestrial Environment, School of Space Science and Technology, Institute of Space Sciences, Shandong University, Weihai, P.R. China. e-mail: zcling@sdu.edu.cn

volcanism) and the regolith formation processes of this unique young mare unit on the lunar farside.

Results

Mineral assemblages and proportions

Mineral component (Fig. 1 and Table 1) and grain size (Supplementary Fig. 2) of the CE-6 lunar soil sample CE6C0300 were performed based on Raman point-counting analysis (see Supplementary Discussion 1 and 2). The results indicate that the CE-6 soil is predominantly composed of plagioclase (46.1 vol %), clinopyroxene (24.4 vol%), and amorphous glass (21.1 vol%), with low proportions of orthopyroxene (2.9 vol%), olivine (1.9 vol%), spinel (1.9 vol %), ilmenite (1.1 vol%), and other minerals (0.8 vol%).

The CE-6 lunar soil contains a significant amount of plagioclase (Fig. 2), which is similar to most of the Apollo 17 mare soils (38.8–52.3 vol%) but lower than the Apollo 16 highland soil materials (49.8–83.9 vol%)[19], possibly contaminated by the ejecta from Chaffee S crater within the Apollo basin. The glass content is relatively low, primarily consisting of feldspathic glass (Table 1) formed by impact events, unlike the basaltic glass predominant in Chang'e-5 (CE-5) soils[21,22]. The CE-6 soil remains at the lower limit of glass content observed in Apollo samples (<30 vol%)[19]. The clinopyroxene content is similar to that of most Apollo mare soils but lower than that of CE-5 lunar soil. Additionally, the CE6C0300 sample is notably depleted in olivine and ilmenite, differing from the previously analyzed CE-5 and Apollo lunar soils[19,21,22], representing an unusual mare unit on the lunar surface.

Fe-Ti-Cr oxides are primarily represented by ilmenite (0.9–1.3 vol%) and spinel (1.3–3 vol%), with the ilmenite Raman peak around 680 cm^{-1} (Fig. 1). Spinel exhibits variable Raman peaks, ranging from 671 cm^{-1} for ulvöspinel to 734 cm^{-1} for chromite with over 70 vol% identified as ulvöspinel, representing late-stage mineral assemblage of parental magma in the CE-6 landing site. A smaller fraction of these spinel grains, relatively rich in magnesium, may represent impact ejecta from small craters within the Apollo basin.

Cristobalite is the primary silica phase in CE-6 soils, with main Raman peaks at 408 cm^{-1} and 228 cm^{-1} (Fig. 1). Low-temperature quartz (<1%) is typically associated with iron-rich pyroxene or plagioclase, displaying main Raman peaks at 458–460 cm^{-1} (Supplementary Fig. 3). Apatite is the dominant phosphate phase in the CE-6 soil, characterized by sharp and distinctive Raman peak at 954–964 cm^{-1} (Supplementary Fig. 4). However, the water peaks of apatite Raman spectra exhibit distinct bands, suggesting various hydration mechanisms, including indigenous OH and solar wind-induced OH on soil particles, which is similar to the contributions observed in the CE-5 samples[23]. Additionally, we identified a minor amount of zircon-rich mineral—tranquillityite, which commonly contains high concentrations of rare earth elements and uranium[24]. Its Raman spectrum is characterized by a broad peak at 735 cm^{-1} (Fig. 1), supporting the amorphous nature from radiation damage by alpha particles[25]. Compared to the CE-5 soil samples, the CE-6 soil contains more sulfide minerals (e.g., troilite) with a main Raman peak at 157 cm^{-1}, which is consistent with the reported 160 cm^{-1} Raman peak[26]. However, this peak could not be used to discriminate between the different sulfide compositions.

Unlike Apollo soils, the CE-6 soil sample contains lower amounts of glass, with glasses being present in the CE-6 soil grain size fractions ranging from <1 μm to several tens of micrometers. The diverse glass Raman spectra indicate variable compositions (Fig. 1), composed of basaltic glass, feldspathic glass, silica glass, and pyroxene glass. The Raman spectra of basaltic glass display two prominent broad peaks at 770 and 970 cm^{-1}. Feldspathic glass also exhibits two broad Raman peaks similar to those of plagioclase, centered at 530 and 990 cm^{-1}. Silica glasses exhibit distinct Raman characteristics, with a single broad peak at 300 cm^{-1}. Notably, the Raman spectra of pyroxene glasses resemble that of pyroxene but exhibit the broadening Raman peaks at 300–400 cm^{-1}, 450–550 cm^{-1}, and 640–690 cm^{-1} (Fig. 1), potentially indicating partially crystallized pyroxene or quench glass on the surface of pyroxene grains.

Silicate mineral chemistries

The primary mafic mineral in the CE-6 soil is pyroxene in terms of the bulk and three subregions, with clinopyroxene being dominant. The pyroxene Raman peaks can be used to determine its chemical composition with an uncertainty of ±10%[27], and most pyroxene (~60 vol%) exhibit Raman peak positions that trend toward the iron-rich endmember, with main peaks at <660 cm^{-1} and <315 cm^{-1} in the ranges of 650–700 cm^{-1} and 300–330 cm^{-1} (Fig. 1 and Supplementary Fig. 5), respectively, indicating more evolved

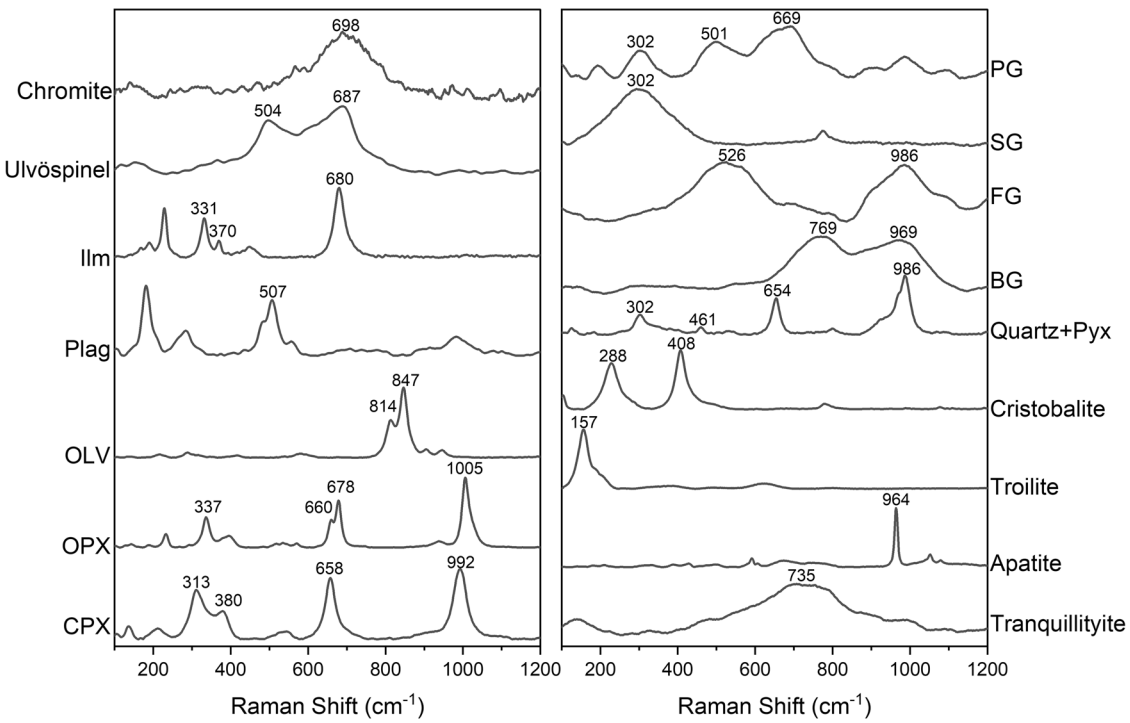

Fig. 1 | Representative Raman spectra with background correction of mineral phases in the CE-6 sample CE6C0300. CPX clinopyroxene, OPX orthopyroxene, Pyx pyroxene, OLV olivine, Plag plagioclase, Ilm ilmenite, BG basaltic glass, FG feldspathic glass, SG silica glass, PG pyroxene glass.

Table 1 | Modal mineralogy (volume%) of CE-6 soil sample CE6C0300

Sample	CE6C0300[1]					CE6C0000[2]			
	Bulk	Region 1	Region 2	Region 3	Average	YJFM00107	YJFM00108	YJFM00109	Average
Method	Raman point-counting (vol%)					XRD (vol%)			
CPX	24.4	28	22.2	23	24.4 ± 2.6	30.3	31.1	27.6	29.7
OPX	2.3	1.3	5.6	2.3	2.9 ± 1.9	3.7	3.8	3.4	3.6
Olivine	2.4	1.7	1.7	1.8	1.9 ± 0.3	0.6	0.2	0.6	0.5
Plagioclase	45	44.9	47	47.3	46.1 ± 1.3	32.9	32.3	32.7	32.6
BG	3.2	1.3	2.6	1.4	2.1 ± 0.9	27.9	28.6	31.8	29.4
FG	14	11.9	13.2	13.5	13.2 ± 0.9				
SG	0.6	0.8	1.3	0.9	0.9 ± 0.3				
PG	3	6.4	4.3	5.9	4.9 ± 1.6				
Ilmenite	1.4	1.7	0.4	0.9	1.1 ± 0.6	1.8	1.5	1.4	1.6
Spinel	2.1	1.7	1.3	2.3	1.9 ± 0.4	0.6	0.2	0.6	0.5
Cristobalite	0.4	0.4	no	no	0.2				
Apatite	0.5	no	no	0.5	0.25				
Quartz	0.1	no	0.4	0.5	0.25 ± 0.2				
Troilite	0.4	no	no	no	0.1				
Plagioclase /Pyroxene	1.7	1.5	1.7	1.9	1.7	1.1	1	1.2	1.1

Reference: 1. This work; 2. Li et al.[13].

CPX clinopyroxene, *OPX* orthopyroxene, *BG* basaltic glass, *FG* feldspathic glass, *SG* silica glass, *PG* pyroxene glass, *no* not observed, *XRD* X-ray diffraction.

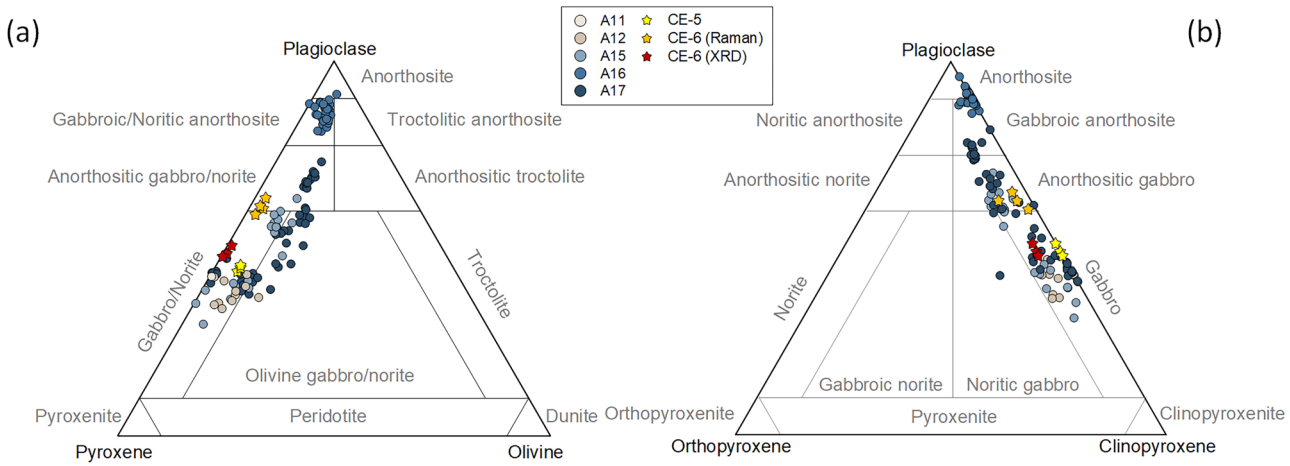

Fig. 2 | Mineral abundance of CE-6 lunar soils compared with Apollo and CE-5 soil samples. a Plagioclase-olivine-pyroxene ternary diagram (vol%) showing the relative abundances of major mineral groups in Apollo, CE-5, and CE-6 soils. **b** Plagioclase-clinopyroxene-orthopyroxene ternary diagram (vol%). Mineralogical data are compiled from Taylor et al.[19] for Apollo soils, Li et al.[22] for CE-5 soils, and Li et al.[13] and this work for CE-6 soils.

characteristics than those found in Apollo and CE-5 basalts[21,28]. Based on the developed calibration formulae[27], the chemical composition of pyroxene ranges from $En_{59}Fs_{22}Wo_{19}$ to $En_4Fs_{81}Wo_{15}$, showing a similar trend to those of CE-5 and Apollo 12 and 15 lunar soils but with a compositional shift toward Fs-rich ferroaugite (Fig. 3). The CE-6 lunar soil contains a significant amount of components in the pyroxene forbidden zone, which typically decompose under lunar surface conditions to form a more stable mineral assemblage of fayalite, hedenbergite, and silica[29]. Additionally, some well-crystallized orthopyroxene have been identified, with main Raman peaks generally trending toward the magnesium-rich endmember, exhibiting a composition range of $En_{37\text{-}66}Fs_{22\text{-}46}Wo_{3\text{-}5}$.

In the CE-6 regolith, the occurrence of olivine is notably scarce, with over 66% being iron-rich olivine ($Fo_{<20}$), characterized by Raman peaks at 805–815 cm^{-1} and 837–847 cm^{-1}. A single high-magnesium olivine ($Fo_{>90}$) was identified, indicative of the ejecta component. The predominant mineral in the CE-6 soil is plagioclase, primarily composed of high-temperature anorthite (51.5–63.1 vol%) and shock-induced anorthite (35.1–44.6 vol%), while low-temperature anorthite (<2 vol%) and Na-Ca plagioclase (<3 vol%) are minimal (Supplementary Fig. 6).

Discussions

Exogenous materials associated with Mg-pyroxene SPA annulus

The CE-6 soils preserve evidence of a mixing process between localized basalts and exogenic ejecta materials (Supplementary Fig. 7). Mineralogically, the primary constituents of the CE-6 soils are plagioclase, pyroxene, and glass (Table 1), with feldspathic glass (13.2 vol%) being the predominant type. This differs from the mineral abundance of CE-6 basalt fragments[30,31]. Despite these differences in mineral abundance, the pyroxene compositions in the CE-6 soils closely resemble those found in the CE-6 basalt, notably containing abundant extremely iron-rich pyroxenes (Fig. 3). The presence of such Fe-rich pyroxenes suggests a distinctive magmatic evolution for CE-6 basalts, markedly different from Apollo mare basalts on the nearside[28]. Recent petrogenetic works have proposed that the CE-6 basalts were sourced from a moderately enriched, KREEP-poor (potassium

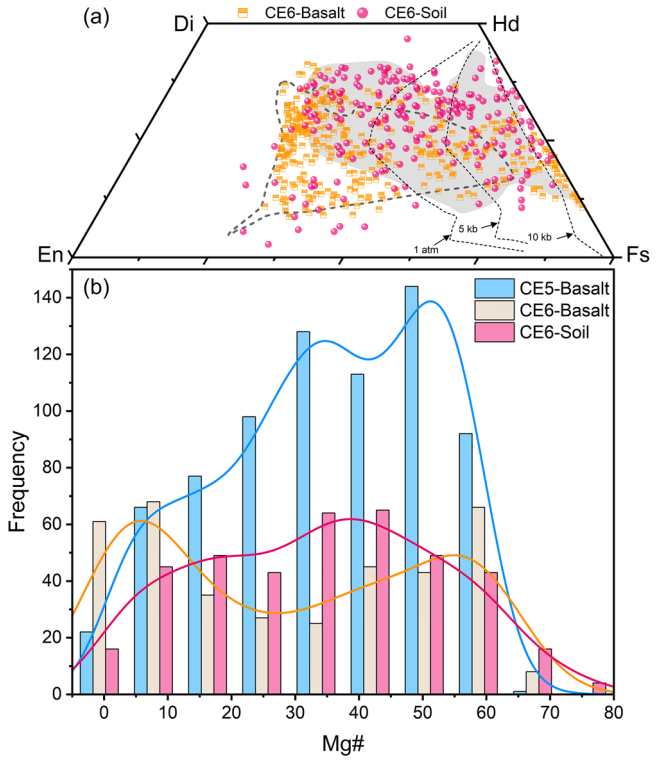

Fig. 3 | Pyroxene composition for the CE-6 soil. Quadrilateral pyroxene compositions (**a**) and Mg# distribution (**b**) for the CE6C0300 sample in comparison with CE-5 basalt[49–53] and CE-6 basalt[31,34]. The gray field and black dashed line indicate the compositional range of CE-5 basalt and Apollo 12 & 15 basalts[28].

(K), rare earth elements (REE), and phosphorus (P)) mantle source that had experienced multiple stages of partial melting and melt extraction[31,32]. The observed iron enrichment in pyroxenes likely reflects extensive fractional crystallization of a Fe-rich melt derived from a hybrid mantle, with crystallization occurring at relatively shallow crustal depths under low-pressure conditions. The notable absence of olivine in the CE-6 soil samples further supports the interpretation that pyroxene crystallized from a progressively evolved melt, consistent with late-stage differentiation and cooling. An alternative possibility is that localized mantle heterogeneities beneath the SPA basin. These may have resulted from earlier impact-induced mixing or the presence of KREEP-poor cumulate zones from the lunar magma ocean, which could have facilitated the generation of Fe-rich, low-degree partial melts with relatively low melting temperatures. This scenario is consistent with both the unusually young eruption age of the CE-6 basalts (~2.8 Ga)[33,34] and the evolved pyroxene chemistry observed in the CE-6 soils.

Given the diverse sources and complex mineralogical characteristics of the exotic ejecta, this work focuses on plagioclase and associated diaplectic glasses in the CE-6 lunar soils to evaluate the proportion of exogenous ejecta. Using the Apollo two-component mixing model[35], the proportion of exotic ejecta in the CE-6 landing site is calculated to be 31–40 vol%. Considering that the dominant feldspathic glass is likely derived from the thermal metamorphism of plagioclase within the exogenous ejecta during the impact process, the mineral abundance of exotic ejecta is determined to be 65–86 vol% plagioclase and 14–35 vol% pyroxene, with a composition ranging from noritic anorthosite to anorthositic norite (gabbro). Assuming that the CE-6 soils are mixtures of local basalts and exogenous ejecta, the compositions of ejecta (Supplementary Table 1) can be derived by deconvolving the published CE-6 soils and basalt data[13] with the estimated ejecta fraction. The derived composition and mineral abundance suggest that ejecta materials have a typically noritic signature (Supplementary Table 2) using CIPW norm calculations. Additionally, uncertainties in the proportion and composition of exogenous materials in CE-6 soils were introduced due to the limited constraints on their bulk compositions and mineralogical properties.

The estimated ejecta thickness at the CE-6 landing site indicates that material from Eratosthenian craters (~40.6 cm) is thicker than that from Chaffee S crater (~16.2 cm)[17]. However, factors such as ejecta deposition efficiency, emplacement chronology, proximity, and ballistic transport dynamics suggest that the thicker ejecta deposits from distant Eratosthenian craters have likely experienced extensive reworking and homogenization over time. In contrast, the Chaffee S crater represents a more recent impact event, contributing relatively fresh ejecta on the top surface layer that has experienced minimal space weathering and lateral mixing. This contrast enhances the likelihood that Chaffee S ejecta is the dominant source of exotic materials at the CE-6 landing site. Furthermore, recent works also support that the primary exogenous ejecta at the CE-6 landing site is sourced from Chaffee S crater[36–38]. Based on the estimated contribution of Chaffee S ejecta as the primary exotic component (>75%) in the returned CE-6 samples, the calculated average composition of the Chaffee S ejecta materials is: 46.0–46.3 wt% SiO_2, 21.0–23.5 wt% Al_2O_3, 6. 9–10.1 wt% FeO, 9.9–11.0 wt % MgO, and 12.5 wt% CaO, with an Mg# range of 63.7–74.0 (Supplementary Table 3). The mineral component of the Chaffee S ejecta is determined to be 63.1–67.2 vol% plagioclase, 3.4 vol% diopside, 25.2–26.6 vol% hypersthene, and 6.8–7.0 vol% olivine (Supplementary Table 4) by the CIPW norm, revealing a noritic composition of the Apollo crater floor.

The Apollo basin is located within the Mg-pyroxene annulus[8], and the Chaffee S crater is highly likely to have ejected Mg-rich materials from the Apollo basin floor to the CE-6 landing site. The returned CE-6 lunar soil reveals a noritic composition of the Mg-pyroxene annulus, which is consistent with previous works suggesting differentiation of the SPA impact melt sheet[39–42], triggering localized magmatic activity. The Mg-pyroxene annulus is notably enriched in plagioclase, while post-SPA impact events may have deposited 20–50% of lunar crustal material back into the SPA basin floor[43,44], enriching the Mg-pyroxene annulus in plagioclase but not obscuring the norite signature of the SPA impact melt sheet differentiation. If the exogenic ejecta from Chaffee S crater is primarily responsible for the CE-6 lunar soils, the plagioclase content (63–67 vol%) of the Mg-pyroxene annulus greatly exceeds the plagioclase content (~25 vol%) in the norite resulting from SPA impact melt sheet differentiation, indicating additional contributions from post-SPA processes or a higher initial Al content in the SPA impact melt. However, petrological models suggest that a higher Al content in the initial melt would not affect the top norite layer, while the addition of exogenic crustal materials would form a thick (~3 km) deep-seated plagioclase-rich layer, consistent with remote sensing observations[8] and the exogenic ejecta in the CE-6 lunar soils. Therefore, the increased plagioclase content in the Mg-pyroxene annulus indicates that additional lunar crustal materials from post-SPA events is introduced from the exterior of SPA. Assuming that the Mg-pyroxene annulus is the top layer of the differentiated SPA impact melt sheet, and that norite exposed by the Chaffee S impact crater at the Apollo basin floor was contaminated by exogenic plagioclase-rich materials, the lunar crust contribution from post-SPA processes would have a plagioclase content of approximately 61–63 vol%. These exogenic materials are likely the lunar crust removed by the SPA impact event and re-ejected during distal (e.g., Imbrium and Orientale) or adjacent (e.g., Apollo and Ingenii) large impact events, ultimately re-depositing into the top norite layer of the differentiated SPA impact melt sheet and forming the plagioclase-rich Mg-pyroxene annulus. In summary, the exogenic ejecta in the CE-6 lunar soil indicates that the Mg-pyroxene annulus is likely a mixture of differentiated norite from the SPA impact melt sheet and re-deposited SPA lunar crust (61–63 vol%).

Alternatively, although previous works have identified ~2.83 Ga mare basalts within the CE-6 soil samples[33,34], it remains unclear whether the noritic signature observed in this work represents a primary lithology or results from compositional mixing between highland materials and mare basalts. In a broader lithological context, the CE-6 soils are likely composed of a complex mixture of materials derived from both the lunar magma ocean

products such as ferroan anorthosite and mare basalts, and secondary ejecta from the SPA basin impact melt, which sampled the noritic upper crust. Regarding the young basalt fragments identified in the CE-6 samples, although their ~2.83 Ga crystallization ages[33,34] are consistent with primary volcanic emplacement, the possibility that some of these units represent recrystallized impact-derived melts derived from localized soils cannot be definitively excluded.

Clues from exotic materials to Apollo basin formation and the SPA geochemistry

Pyroxene compositional mapping shows that the remainder of central SPA is dominated by Mg-rich pyroxenes across a wide range of crater sizes, defining a continuous Mg-pyroxene annulus[8]. Surrounding this is a heterogeneous annulus with localized Mg-pyroxene deposits set in low-mafic materials. The ubiquity of Mg-pyroxene in some craters implies laterally and vertically extensive Mg-pyroxene-bearing lithologies, as deep-seated impact melt and breccia excavated by the basin-forming event, and suggests these Mg-rich phases were the primary constituents of the SPA impact melt. By contrast, the Apollo basin floor situated within the Mg-pyroxene annulus exhibits only sporadic Mg-pyroxene exposures, most prominently at the Chaffee crater. In terms of lithological distribution, the Apollo basin floor is largely composed of anorthositic norite, with minor noritic anorthosite confined to the northeast and a few northern patches[45]. Our results indicate that the CE-6 sampling site predominantly received ejecta from Chaffee S crater within the Apollo basin, characterized by a noritic signature (Mg#: 63.7–74.0; plagioclase: ~63–67 vol %). We attribute this to stratified crystallization in the SPA impact melt sheet, where an upper noritic cumulate layer rich in pyroxene and plagioclase overlies a deeper horizon enriched in Mg-bearing phases such as pyroxene and olivine. Because the Apollo basin was contaminated by ejecta deposits from later impact events which excavate only its upper cumulate zone of this melt sheet, its floor exposed these noritic cumulates, reflecting the top differentiation layer of the SPA impact melt. Moreover, we find that the surrounding Mg-pyroxene annulus not only records primary melt differentiation but has been overprinted by later impact events (e.g., Oppenheimer and Orientale basin) that reworked and redeposited crustal materials, contributing to an enhanced plagioclase abundance. This hybrid stratigraphy shaped by both primary differentiation and secondary exogenous reworking explains the co-enrichment of Mg# and plagioclase and the resulting high-Mg noritic mineral assemblage on the Apollo basin floor.

Remote sensing data from Lunar Prospector reveal a broad enhancement in Th across the SPA basin relative to the surrounding farside highlands[39]. However, the Apollo basin, located near the rim of the SPA basin, exhibits a marked Th depletion (<2.5 ppm) with local minima (<2.0 ppm) concentrated in its peak ring and impact melt sheet[9]. These values are consistent with the incompatible-element-depleted nature of the CE-6 soils (~0.9 ppm) and recognized norite fragments (<0.1 ppm in pyroxene and plagioclase)[13,46], indicating that the Apollo basin floor is composed of deep crustal lithologies lacking KREEP components, likely representing products of impact melt differentiation with minimal enrichment in incompatible elements. The FeO distribution in the SPA basin interior is generally elevated (~10–15 wt%) compared to the SPA exterior (~7–10 wt%)[39]. However, the FeO concentrations in the CE-6 exotic materials (6.9–10.1 wt%) and norite fragments (5.8 ± 2.1 wt%)[46] fall at the lower end of this range, suggesting a dominance of moderately ferroan noritic lithologies rather than more mafic or ultramafic assemblages. This supports interpretations that the Apollo basin floor and by extension, portions of the SPA basin interior are composed predominantly of Mg-rich, low-Fe, crustally derived materials that have been subsequently modified by post-SPA impact processes and the re-deposition of plagioclase-rich ejecta. The high Mg# values of exotic materials within the CE-6 samples further support a crustal origin, consistent with a low-Fe, high-Mg silicate assemblage typical of differentiated norites formed by crystallization of the SPA impact melt sheet. The plagioclase abundance in the Mg-pyroxene annulus (~63–67 vol%) far exceeds that expected for differentiated impact melt (~25 vol%), indicating substantial contributions from reworked upper crustal materials delivered during later large impacts (e.g., Oppenheimer, Orientale), which enriched the region in plagioclase while preserving the underlying noritic signature. Collectively, the CE-6 sample data and global geochemical maps suggest that the SPA basin interior is compositionally stratified, characterized by (1) low Th abundance in the inner basin and melt sheet except northwest quadrant (e.g., craters Birkeland and Oresme V), indicating incompatible-element-poor lithologies; (2) moderate FeO contents due to deep excavation of Fe-rich source, impact-melt fractionation, and secondary reworking by later impact events; (3) elevated Mg# and plagioclase enrichment in the Mg-pyroxene annulus, indicative of both primary melt differentiation and secondary reworking of anorthositic crust. These results enhance our understanding of the SPA geochemistry as a heterogeneous assemblage of differentiated impact melt and re-accreted crustal materials. This further suggests that the deep noritic layer likely formed through large-scale differentiation of the SPA impact melt sheet, later overprinted by post-SPA impact processes.

Future missions aiming to sample mantle materials in the SPA basin or similar deep basins should therefore consider targeting central peaks or peak rings of large, complex craters that formed later within the SPA basin. These central uplift structures are more likely to expose deeper lithologies, including possible lower crustal or upper mantle materials. In addition, landing sites located in regions with minimal post-SPA crustal reworking and thinner crustal cover (e.g., near crater central uplifts like Leibnitz or Finsen) may provide better access to deeper lithologies.

Evolution pathway of unique farside mare soils

Lunar surface soils are classified as immature, sub-mature, and mature[47]. Immature soils are primarily derived from ejecta of large impact craters. Frequent micrometeorite bombardment and solar wind implantation then facilitate the transformation of fresh ejecta (containing various-size rock fragments) into uniform fine-grained material. This evolution occurs through processes such as fragmentation, volatilization, melting, and agglutination. As a result, the regolith becomes sub-mature and mature regolith, with a notable increase in the content of agglutinatic glass[20]. The CE-6 landing site is mainly covered by ejecta excavated by a small, heavily degraded impact crater approximately 50 meters in diameter (Crater 27). Additional contributions likely come from basaltic ejecta associated with a nearby, eroded crater about 30 meters in diameter (Crater 29, Supplementary Fig. 8). After the formation of the CE-6 basalt unit (~2.8 Ga)[33,34], the Chaffee S cratering event within the Apollo basin[17], ejected impact melt that heated the underlying basaltic regolith to temperatures between 700–800 °C (Supplementary Discussion 3). This event also incorporated 30–40 vol% magnesium-rich ($Mg\#_{>70}$) noritic materials into the local regolith, contributing to plagioclase amorphization and quartz metamorphism. This process initiated the development of the distinctive mineralogical characteristics with abundant plagioclase and amorphous glass observed in the CE-6 regolith.

During the subsequent hundreds of millions of years, continuous micrometeorite bombardment gradually pulverized and redeposited the fresh ejecta, which mixed with the existing weathered basaltic regolith, further facilitating the accumulation of amorphous glass. Subsequently, small impact events (<50 m in diameter, Supplementary Fig. 8) around the landing site excavated and exposed subsurface ejecta rich in coarse-grained Chaffee S materials with high-Mg nature, through both lateral transport and mixing processes. This replenishment of coarse material (>30%) was reintroduced into the soil evolution process by impact comminution of the underlying megaregolith. Continuous micrometeorite bombardment and solar wind implantation fragmented and reduced the supplemented large particles, contributing to the regolith melting and forming agglutinatic glass and metallic iron. This process was further complemented by coarse material from surrounding small impact events. This resulted in highly uniform fine-grained soils at the CE-6 landing site, with the identified fraction of large particles (>30%) indicating that the rate of fine-graining and replenishment from extraneous coarse-grained materials had not yet reached equilibrium[20]. While fine-graining continues over extended timescales, equilibrium remains challenging to achieve due to the recurrent impact events that introduce coarse-grained materials. The rate of fine-

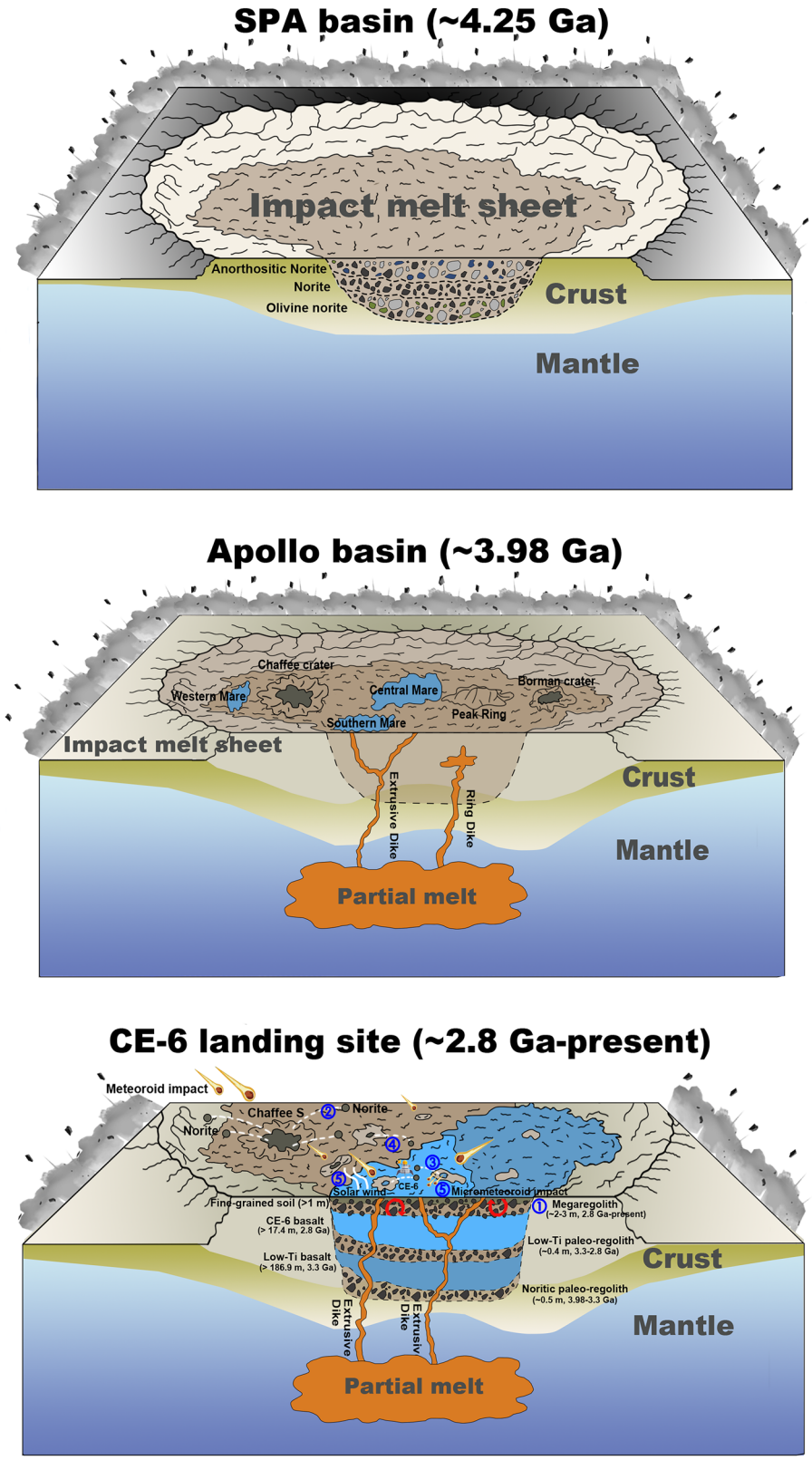

Fig. 4 | The geological processes involved in regolith evolution at the CE-6 landing site. The SPA impact melt sheet formed around 4.25 Ga[46] and experienced fractional crystallization, producing stratified noritic layers. At ~3.98 Ga[54], the Apollo impact event excavated these differentiated products. Around the same time, contemporaneous large-scale basin-forming events in the lunar highlands re-deposited crustal materials into the SPA basin floor. Subsequent impacts within the SPA dispersed noritic ejecta across the Apollo basin floor. This era also marked the onset of multiple episodes of mare volcanism. By ~3.3 Ga, low-Ti mare basalts were emplaced in the southern portion of the basin, followed by the accumulation of a thin paleo-regolith layer. At ~2.8 Ga, emplacement of the CE-6 basalts occurred. The overlying regolith subsequently evolved through a range of surface processes, including (1) the development of an early megaregolith; (2) physical mixing with noritic ejecta from Chaffee S crater; (3) fragmentation of fresh ejecta rocks by small-scale impacts at the landing site; (4) episodic replenishment of coarse regolith from nearby craters; and (5) progressive space weathering. Subsurface stratigraphy in the CE-6 landing site is modified from Gou et al.[55].

graining has not yet exceeded the influx of larger, coarse-grained particles. This imbalance may be attributed to the relatively young age of the CE-6 zone, which is likely still experiencing active replenishment from nearby ejecta or continuous impact events. Thus, the majority of agglutinates and comminuted debris in the sample CE6C0300 with the mature nature are produced by micrometeoroid bombardment affecting the uppermost few millimeters of the lunar regolith.

Based on an unimodal grain size distribution and fine-grained nature of the CE-6 soil sample, in association with the geological context, the evolution pathway of the CE-6 lunar soils primarily involves (Fig. 4): (1) formation of an early regolith layer due to space weathering process over hundreds of millions of years after the formation of the CE-6 basalt unit at ~2.8 Ga[33,34]; (2) physical mixing of existing soils and Mg-rich noritic ejecta from distant large impact craters, represented by the Chaffee S cratering

event[17]; (3) fragmentation of fresh ejecta rocks into coarse megaregolith by small impact events at the landing site, accompanied by the accumulation of amorphous glass (20 ~ 30 vol%); (4) subsequent replenishment of coarse regolith through nearby small impact events while fine-graining of the regolith occurs with low-temperature shock metamorphism (<31.4 GPa, Supplementary Discussion 3); (5) long-term space weathering processes facilitating the accumulation of fine-grained soils, agglutinatic glass, and metallic iron. Therefore, the early evolution of the regolith at the CE-6 landing site primarily involved a physical mixing process, while late-stage processes were characterized by a combination of physical mixing and space weathering effects.

Online methods

CE-6 samples preparation. The CE-6 samples are categorized into scooped and drill core samples. In this work, we utilized the CE-6 lunar soil sample CE6C0300YJFM001 (hereinafter abbreviated as CE6C0300). Approximately 1 g of lunar soil was transferred into a petri dish (about 10 cm in diameter) that had been cleaned with ethanol (99.999% purity), and the surface (3 cm × 2.4 cm, Supplementary Fig. 1) was subsequently flattened to facilitate Raman spectroscopic analysis.

Analytical methods. Raman spectroscopic analysis of lunar soil sample CE6C0300 was carried out using a Renishaw Raman spectrometer at Shandong University, Weihai, with a 532-nm green laser (89 mW) as the excitation source[21]. The spectral range was set between 50 and 4000 cm^{-1}, with a resolution exceeding 1 cm^{-1} and a repeatability of ±0.2 cm^{-1}. An optical image of the CE6C0300 sample was initially captured using a 5X (NA = 0.12) objective lens, followed by more detailed mineral analysis and grain size (Supplementary Fig. 2) with a 50X (NA = 0.5) long-working-distance objective, producing a laser beam diameter of approximately 2.5 μm. Before Raman measurements, this system was calibrated for absolute wavelength using the emission lines of a standard Ne lamp manufactured by the Renishaw, with a monocrystalline silicon reference peak at 520.7 cm^{-1} employed for calibrating the Raman shift, ensuring peak accuracy of ±0.2 cm^{-1}.

A Raman point-counting analysis was applied to lunar soil CE6C0300, with an equally spaced grid of 1 mm covering a total of 916 points. In addition, three subregions (regions 1, 2, and 3) were selected for high-resolution mineralogical analysis, using a 0.2 mm spacing and collecting 225 spectra from each subregion. The experimental conditions were set to a laser power of ~0.89 mW, 20 s exposure time, and two accumulation iterations. For heat-sensitive minerals, including iron oxides and sulfides, lower-power laser settings were used to prevent thermal damage during the analysis. In addition, we conducted replicate measurements on multiple grains of the same mineral to assess reproducibility. The standard deviation of peak positions among these replicates was consistently <1 cm^{-1}, supporting the robustness of the point-counting approach.

In this work, the collected Raman spectral peaks were processed using Savitzky-Golay (SG) smoothing functions for minimizing background noise, polynomial fitting for subtracting baseline, and spectral deconvolution employing a mixed Gaussian-Lorentzian algorithm. This method is able to identify the main Raman peaks for pyroxene and olivine. To estimate silicate mineral chemistry (e.g., Fo content in olivine and En-Fs-Wo in pyroxene), we applied empirical calibrations from well-established literature[27,48], which yield estimated uncertainties of ±10 mol% for olivine Fo content and ±10 for pyroxene En-Fs-Wo. While these estimates do not replace quantitative elemental analysis, they provide reproducible and non-destructive compositional constraints that are consistent with the precision of Raman-based geochemical assessments.

Data availability

The data resulting from this work are provided in the Article and Supporting Information. LROC NAC data were downloaded from the Planetary Data System (https://pds-geosciences.wustl.edu/). Data behind figures are available at figshare (https://figshare.com/s/d3c8b0bd04241be35b58).

Received: 14 January 2025; Accepted: 4 June 2025;
Published online: 06 July 2025

References

1. Lawrence, D. et al. Iron abundances on the lunar surface as measured by the Lunar Prospector gamma–ray and neutron spectrometers. *J. Geophys. Res. Planets* **107**, 13-11-13-26 (2002).
2. Lawrence, D. et al. Small–area thorium features on the lunar surface. *J. Geophys. Res. Planets* **108**, 5102 (2003).
3. Pieters, C. M., Tompkins, S., Head, J. & Hess, P. Mineralogy of the mafic anomaly in the South Pole–Aitken Basin: Implications for excavation of the lunar mantle. *Geophys. Res. Lett.* **24**, 1903–1906 (1997).
4. Pieters, C., Head, J., Gaddis, L., Jolliff, B. & Duke, M. Rock types of South Pole–Aitken basin and extent of basaltic volcanism. *J. Geophys. Res. Planets* **106**, 28001–28022 (2001).
5. Potter, R., Kring, D., Collins, G., Kiefer, W. & McGovern, P. Estimating transient crater size using the crustal annular bulge: Insights from numerical modeling of lunar basin–scale impacts. *Geophys. Res. Lett.* **39**, L18203 (2012).
6. Yamamoto, S. et al. Possible mantle origin of olivine around lunar impact basins detected by SELENE. *Nat. Geosci.* **3**, 533–536 (2010).
7. Pasckert, J. H., Hiesinger, H. & van der Bogert, C. H. Lunar farside volcanism in and around the South Pole–Aitken basin. *Icarus* **299**, 538–562 (2018).
8. Moriarty Iii, D. & Pieters, C. The character of South Pole–Aitken Basin: Patterns of surface and subsurface composition. *J. Geophys. Res. Planets* **123**, 729–747 (2018).
9. Moriarty, I. I. I. et al. Evidence for a stratified upper mantle preserved within the South Pole–Aitken Basin. *J. Geophys. Res. Planets* **121**, e2020JE006589 (2021).
10. Melosh, H. et al. South Pole–Aitken basin ejecta reveal the Moon's upper mantle. *Geology* **45**, 1063–1066 (2017).
11. Lin, H. et al. Olivine-norite rock detected by the lunar rover Yutu-2 likely crystallized from the SPA-impact melt pool. *Natl. Sci. Rev.* **7**, 913–920 (2020).
12. Yang, W., He, Y., Qian, Y. & Yue, Z. Scientists eager for Chang'e-6 lunar farside samples to bring new discoveries. *Innov* **5**, 100660 (2024).
13. Li, C. et al. Nature of the lunar far-side samples returned by the Chang'E-6 mission. *Natl. Sci. Rev.* **11**, nwae328 (2024).
14. Zeng, X. et al. Landing site of the Chang'e-6 lunar farside sample return mission from the Apollo basin. *Nat. Astron* **7**, 1188–1197 (2023).
15. Qian, Y. et al. Long-lasting farside volcanism in the Apollo basin: Chang'e-6 landing site. *Earth Planet. Sci. Lett.* **637**, 118737 (2024).
16. Luo, F. et al. The Production Population of Impact Craters in the Chang'E-6 Landing Mare. *Astrophys. J. Lett.* **974**, L37 (2024).
17. Yue, Z. et al. Geological context of the Chang'e-6 landing area and implications for sample analysis. *Innov* **5**, 100663 (2024).
18. Heiken, G. Petrology of lunar soils. *Rev. Geophys.* **13**, 567–587 (1975).
19. Taylor, G. J. et al. Modal analyses of lunar soils by quantitative X-ray diffraction analysis. *Geochim. Cosmochim. Acta* **266**, 17–28 (2019).
20. McKay, D. S., Fruland, R. M. & Heiken, G. H. Grain size and the evolution of lunar soils. In *Proceedings of the 5th Lunar Science Conference*. 887-906 (Pergamon, 1974).
21. Cao, H. et al. A Raman spectroscopic and microimage analysis perspective of the Chang'e–5 lunar samples. *Geophys. Res. Lett.* **49**, e2022GL099282 (2022).
22. Li, C. et al. Characteristics of the lunar samples returned by the Chang'E-5 mission. *Natl. Sci. Rev.* **9**, nwab188 (2022).
23. Liu, J. et al. Evidence of water on the lunar surface from Chang'E-5 in-situ spectra and returned samples. *Nat. Commun.* **13**, 3119 (2022).
24. Lovering, J. et al. Tranquillityite: A new silicate mineral from Apollo 11 and Apollo 12 basaltic rocks. In *Proceedings of the 2st Lunar Science Conference*. 39 (Pergamon, 1971).

25. Gatehouse, B., Grey, I., Lovering, J. & Wark, D. Structural studies on tranquillityite and related synthetic phases. In *Proceedings of the 8th Lunar Science Conference*. 1831-1838 (Pergamon, 1977).
26. Avril, C. et al. Raman spectroscopic properties and Raman identification of CaS-MgS-MnS-FeS-Cr_2FeS_4 sulfides in meteorites and reduced sulfur-rich systems. *Meteorit. Planet. Sci.* **48**, 1415–1426 (2013).
27. Wang, A., Jolliff, B. L., Haskin, L. A., Kuebler, K. E. & Viskupic, K. M. Characterization and comparison of structural and compositional features of planetary quadrilateral pyroxenes by Raman spectroscopy. *Am. Mineral.* **86**, 790–806 (2001).
28. Papike, J. J., Hodges, F. N., Bence, A., Cameron, M. & Rhodes, J. Mare basalts: Crystal chemistry, mineralogy, and petrology. *Rev. Geophys.* **14**, 475–540 (1976).
29. Lindsley, D. H. Pyroxene thermometry. *Am. Mineral.* **68**, 477–493 (1983).
30. Che, X. et al. Isotopic and compositional constraints on the source of basalt collected from the lunar far side. *Science*, **387**, 1306–1310 (2025).
31. Yin, C. et al. Petrogenesis of Chang'e-6 Basalts and Implication for the Young Volcanism on the Lunar Farside. *Astrophys. J. Lett.* **981**, L2 (2025).
32. Shen, D. et al. Petrogenesis of Chang'E-6 basalts and implication for multi-episode volcanism in the lunar farside basin. *Earth Planet. Sci. Lett.* **659**, 119335 (2025).
33. Zhang, Q. W. et al. Lunar farside volcanism 2.8 billion years ago from Chang'e-6 basalts. *Nature* https://doi.org/10.1038/s41586-024-08382-0 (2024).
34. Cui, Z. et al. A sample of the Moon's far side retrieved by Chang'e-6 contains 2.83-billion-year-old basalt. *Science* **386**, 1395–1399 (2024).
35. Korotev, R. L. Mixing levels, the Apennine Front soil component, and compositional trends in the Apollo 15 soils. *J. Geophys. Res. Solid Earth* **92**, E411–E431 (1987).
36. Gou, S. et al. Complex basalt evolution in the Chang'e-6 landing area. *Earth Planet. Sci. Lett.* **648**, 119091 (2024).
37. Su, Y., Xu, L., Zhu, M.-H. & Cui, X.-L. Composition and Provenance of the Chang′ e-6 Lunar Samples: Insights from the Simulation of the Impact Gardening Process. *Astrophys. J. Lett.* **976**, L30 (2024).
38. Xu, L., et al. Chronology, local stratigraphy, and foreign ejecta materials at the Chang'e-6 landing site: Constraints on the provenance of samples returned from the Moon's farside. *Geophys. Res. Lett.* **51**, e2024GL111311 (2024).
39. Hurwitz, D. M. & Kring, D. A. Differentiation of the South Pole–Aitken basin impact melt sheet: Implications for lunar exploration. *J. Geophys. Res. Planets* **119**, 1110–1133 (2014).
40. Nakamura, R. et al. Ultramafic impact melt sheet beneath the South Pole–Aitken basin on the Moon. *Geophys. Res. Lett.* **36**, L22202 (2009).
41. Uemoto, K. et al. Evidence of impact melt sheet differentiation of the lunar South Pole-Aitken basin. *J. Geophys. Res. Planets* **122**, 1672–1686 (2017).
42. Vaughan, W. M. & Head, J. W. Impact melt differentiation in the South Pole-Aitken basin: Some observations and speculations. *Planet. Space Sci.* **91**, 101–106 (2014).
43. Petro, N. E. & Pieters, C. M. Surviving the heavy bombardment: Ancient material at the surface of South Pole–Aitken Basin. *J. Geophys. Res. Planets* **109**, E06004 (2004).
44. Petro, N. & Pieters, C. Modeling the provenance of the Apollo 16 regolith. *J. Geophys. Res. Planets* **111**, E09005 (2006).
45. Guo, D. et al. Geological investigation of the lunar Apollo basin: from surface composition to interior structure. *Earth Planet. Sci. Lett.* **646**, 118986 (2024).
46. Su, B. et al. South Pole–Aitken massive impact 4.25 billion years ago revealed by Chang'e-6 samples. *Natl. Sci. Rev.*, **12**, nwaf103 (2025).
47. Morris, R. V. The surface exposure/maturity/of lunar soils-Some concepts and Is/FeO compilation. In *Lunar and Planetary Science Conference Proceedings*. 2287-2297 (Pergamon, 1978).
48. Kuebler, K. E., Jolliff, B. L., Wang, A. & Haskin, L. A. Extracting olivine (Fo–Fa) compositions from Raman spectral peak positions. *Geochim. Cosmochim. Acta* **70**, 6201–6222 (2006).
49. Che, X. et al. Age and composition of young basalts on the Moon, measured from samples returned by Chang'e-5. *Science* **374**, 887–890 (2021).
50. Tian, H.-C. et al. Non-KREEP origin for Chang'e-5 basalts in the Procellarum KREEP Terrane. *Nature* **600**, 59–63 (2021).
51. Jiang, Y., Li, Y., Liao, S., Yin, Z. & Hsu, W. Mineral chemistry and 3D tomography of a Chang'E 5 high-Ti basalt: implication for the lunar thermal evolution history. *Sci. Bull.* **67**, 755–761 (2022).
52. He, Q. et al. Detailed petrogenesis of the unsampled Oceanus Procellarum: The case of the Chang'e-5 mare basalts. *Icarus* **383**, 115082 (2022).
53. Luo, B. et al. The magmatic architecture and evolution of the Chang'e-5 lunar basalts. *Nat. Geosci.* **16**, 301–308 (2023).
54. Ivanov, M. et al. Geologic history of the northern portion of the South Pole-Aitken basin on the Moon. *J. Geophys. Res. Planets* **123**, 2585–2612 (2018).
55. Gou, S. et al. Thin basaltic regolith at the Chang'e-6 landing site. *Earth Planet. Sci. Lett.* **655**, 119266 (2025).

Acknowledgements

We were allocated the CE-6 sample by the China National Space Administration. This work was supported by the fundings from the National Natural Science Foundation (42441804, 42402231, 123B2046, 42241107, 42441817), Postdoctoral Fellowship Program of CPSF (GZC20231431), the China Postdoctoral Science Foundation (2024M761786), National Key Research and Development Program of China (2022YFF0711400, 2022YFF0503100), Geological Survey of China (DD20221645, DD20230007), and the Instrument Improvement Funds of Shandong University Public Technology Platform (ts20230113). We thanks three reviewers for suggestive comments. This is the SDU-CPS publication #175.

Author contributions

Z.L. conceptualized this research. H.C. performed the data analyses and wrote the initial manuscript. H.C., J.C., X.L., J.K., C.Y., C.L., H.Q., and Y.X. contributed to the preparation and spectral measurements of CE-6 soil samples. X.F., L.Q., J.C., X.L., and Z.L. contributed to the geological interpretations of the data. All authors participated in the discussion of the results, data interpretation and paper editing.

Competing interests

The authors declare no competing interests.

Additional information

Supplementary information The online version contains supplementary material available at https://doi.org/10.1038/s43247-025-02441-8.

Correspondence and requests for materials should be addressed to Zongcheng Ling.

Peer review information *Communications Earth and Environment* thanks Yash Srivastava and the other, anonymous, reviewer(s) for their contribution to the peer review of this work. Primary Handling Editors: Ke Zhu, Joseph Aslin.